


ARTICLE OPEN

Vapor dealloying of ultra-thin films: a promising concept for the fabrication of highly flexible transparent conductive metal nanomesh electrodes

Adrien Chauvin¹, Willigis Xia Cha Heu¹, Joze Buh^{2,3}, Pierre-Yves Tessier¹  and Abdel-Aziz El Mel¹

The booming market of flexible electronic displays has urged the development of highly flexible transparent conductive electrodes (FTCE)^{1–3} with the ability to replace indium tin oxide (ITO) thin films routinely used as transparent conductive electrodes in photoelectronic devices. The high cost of indium and the poor mechanical stability of ITO under deformation are the main driving forces behind the development of this research area.⁴ The use of metal nanomeshes as FTCE is a promising concept with a real potential to substitute ITO in photoelectronic devices.^{5,6} However, the development of a low-cost fabrication approach allowing producing metal nanomesh electrodes with competitive prices and a high performance remains a real bottleneck for the photoelectronic industry. In this paper, we report on a robust approach very easy to implement allowing producing highly flexible metal nanomesh electrodes with high performance at a very low cost. This approach lies on a concept consisting in applying dealloying process to ultra-thin Au-Cu alloy thin films using acidic vapors instead of a liquid phase as routinely done in the literature. Using an appropriate procedure, the nanomeshes can be transferred to any planar or curved support where they can serve as a FTCE. As a proof of concept, we demonstrate that using this approach, one can easily fabricate gold nanomesh electrodes transferred onto polyethylene terephthalate (PET) film surface with 79% of transmittance and a sheet resistance as low as $44 \Omega \square^{-1}$ while maintaining exceptional stability under severe mechanical deformations.

npj Flexible Electronics (2019)3:5; <https://doi.org/10.1038/s41528-019-0049-1>

INTRODUCTION

Transparent conductive electrodes (TCEs) represent an essential element in various photoelectronic devices including smartphones, tablets, flat panel displays, and notebooks.¹ These products show market tendencies toward large-scale and thin devices, low power consumption, low cost, robustness against mechanical shocks and deformation and most essentially flexibility (including bendable, stretchable, and foldable types).² The poor resistance of touch-screens against mechanical shocks remains an unsolved bottleneck for the photoelectronic industries. The fragility originates from the use of non-flexible materials such as indium tin oxide (ITO) and cover glass to manufacture the screens. Although ITO is known to exhibit an excellent performance (transmittance in the visible range exceeding 90% and a sheet resistance as low as $10 \Omega \square^{-1}$),⁷ it is extremely brittle, barely flexible and expensive. Remedying the fragility of photoelectronic devices requires upgrading the current technology to a new level by replacing ITO on the glass by highly flexible TCEs (FTCEs) on polymers such as polyethylene terephthalate (PET) or polydimethylsiloxane (PDMS).^{3,4,8}

Driven by the needs of this booming and highly competitive market, the scientific community has explored over the last few years a vast multitude of technologies including silver nanowires,^{9–11} metal grids,¹⁰ carbon nanotubes,¹² graphene,^{13,14} nanotroughs,^{15,16} conductive polymers^{17,18} and metal nanomeshes^{5,6} suitable for the development of flexible screens. Metal

nanomeshes are of particular interest since they revealed very high optoelectronic performances (high transmittance in the visible range and low sheet resistance) comparable to those of ITO on flexible substrates with a capacity to absorb a large strain while keeping a low sheet resistance,^{8,19} in addition, they exhibit several advantages compared to the other cited alternatives.²⁰ In brief, a nanomesh can be described as a network of interconnected metal nanoligaments allowing avoiding the drop in electrical conductivity encountered in case of silver nanowires due to the high wire-to-wire contact resistance.¹⁹ The ultrahigh flexibility of the material originating from such a particular architecture allows the electrode to accommodate strong external mechanical deformation up to 160% strain with only modest change in sheet resistance in the case of gold nanomeshes.⁵

In addition to their excellent optoelectronic performance, the development of a mass production and a low-cost fabrication process of metal nanomeshes is a key requirement for a successful substitution of ITO by metal nanomeshes. For this reason, the race toward the development of relevant and cost-effective fabrication approaches of metal nanomeshes, suitable for mass production on the industrial scale, is still running. Although several fabrication approaches of metal nanomeshes were reported so far in the literature, however, the production cost on the industrial scale of such electrodes is still not competitive enough to replace ITO.^{21–24} For instance, Guo et al.⁵ have developed an approach, based on grain boundary lithography, to fabricate highly flexible gold (Au)

¹Institut des Matériaux Jean Rouxel, IMN, Université de Nantes, CNRS, 2 rue de la Houssinière B.P. 32229, 44322 Nantes cedex 3, France; ²Jožef Stefan Institute, Complex matter department, Jamova cesta 39, 1000 Ljubljana, Slovenia and ³Center of Excellence on Nanoscience and Nanotechnology Nanocenter, Jamova 39, 1000 Ljubljana, Slovenia
Correspondence: Pierre-Yves Tessier (pierre-yves.tessier@cnrs-imn.fr)

Received: 15 June 2018 Accepted: 1 February 2019

Published online: 07 March 2019

nanomesh electrodes with a transmittance of 82.5% and a sheet resistance as low as $21 \Omega \square^{-1}$. Although the achieved performances are remarkable, the high cost of the indium mask involved in their process remains a significant barrier for the production of low-cost nanomesh electrodes on the industrial scale. Another approach has been suggested by Jang et al.⁶ who showed how by direct deposition of platinum by physical vapor deposition on anodized aluminum oxide (AAO) membranes one can produce platinum nanomesh electrodes with a relatively fair performance. In addition to the fact that such Pt nanomeshes exhibit performances (70% at 550 nm and $71 \Omega \square^{-1}$) well below the ones of the electrodes demonstrated by Guo et al.,⁵ the process presents a major drawback related to the difficulty of producing AAO templates in a homogeneous manner over a large scale mandatory for the coverage of the screens of smartphones or tablets.

RESULTS

Here we report on a very efficient fabrication approach of highly flexible and transparent metal nanomesh electrodes easy to implement and suitable for industrial use (Fig. 1a). The novelty of the process lays in the use of “vapor dealloying”²⁵ which is, in itself, a real breakthrough in this research area compared to classical dealloying in liquid phase reported in the literature since the 1960s.²⁶ For the proof of concept, we selected gold-copper (Au-Cu) alloy as a model system to prepare highly flexible gold nanomesh electrodes. At first, an ultra-thin film (thickness between 5 and 20 nm) of Au-Cu alloy is deposited on a glass substrate with a size of 24×40 mm by magnetron co-sputtering of gold and copper targets. In the second step, the alloy film is exposed to the vapors of concentrated nitric acid (16 mol L^{-1}) to leach softly and preferentially copper from the alloy and forms gold interconnected nanoligaments laying on the substrate surface.

During the exposure of the film to the acidic vapors, we remarked that the color and transparency of the film evolves as the dealloying process proceeds in time (Fig. 1b). While the Au-Cu film exhibits a reddish color (representative of copper in the Au-Cu alloy) during the early stage of dealloying, its color turns into brownish during the mid-stage (between 1 and 20 min according to the Au-to-Cu ratio in the alloy layer) due to the formation of $\text{Cu}(\text{NO}_3)_2$ over the surface as confirmed by X-ray photoelectron spectroscopy (Fig. S2). By the end of the dealloying process, the sample becomes transparent and it exhibits an insulating behavior. When examined glass surface under the optical microscope (Fig. 1c), we identified the presence of micropatches clearly separated from each other by microcracks (Fig. S3). Each micropatch is constituted of interconnected nanoligaments. The mean micropatch area is about $1000 \mu\text{m}^2$, the presence of microcracks is attributed to the very high tensile stress generated during the dealloying process.^{27,28}

Applying dealloying using acidic vapors is mandatory for a successful fabrication and transfer of the electrode. More precisely, if the dealloying process is applied in liquid phase by a simple immersion of an Au-Cu ultra-thin film on glass substrate in nitric acid,²⁹ according to the concentration of Au in the alloy and the thickness, the layer can either delaminates and agglomerates during the immersion in the acidic solution (SM1) or survive the acid attack without any degradation (SM2).^{30,31} In the latter case, however, the obtained nanomeshes were found to be electrically insulating due to the presence of microcracks in the nanomesh. In addition, during the transfer onto a flexible substrate, the nanomesh tends to agglomerate (SM3 and SM4). Even by adding an adhesion layer (e.g., chromium or titanium) underneath the ultra-thin Au-Cu layer (solution adopted in our previous work in case of thin films³²), the Au-Cu ultra-thin layer was found to regularly delaminates upon immersion in the acidic solution; this has been tested for different nitric acid concentrations down to 7 mol L^{-1} . Substituting the glass by a polymer substrate allowed

overcoming the delamination issue but the obtained nanomeshes were electrical insulating. When examined using SEM, one can clearly notice the presence of microcracks dividing the nanomesh into isolated micropatches (Fig. S1a). These microcracks result from the high tensile stress generated within the material during the dealloying process. In addition, each single micropatch is constituted of nanoligaments which are physically disconnected from each other (Fig. S1b). Instability issues were also noticed during the aging of the nanomesh resulting in the transformation of the nanoligaments into nanospheres. Among all the strategies we explored so far, applying dealloying using the vapors of nitric acid was the most suitable one to overcome the delamination and agglomeration issues (SM5). This is probably related to the reduced volume of acid used to dealloy the material. In brief, during the vapor dealloying process, the acidic vapors condense over the sample surface and form an ultra-thin layer of concentrated nitric acid serving as a medium for the preferential leaching of copper from the alloy. In the course of dealloying, the gold atoms undergo a surface diffusion process resulting in the formation of a planar gold skeleton consisting of interconnected nanoligaments. It is assumed that the fundamental mechanisms of the dealloying process applied in the “vapor phase” and in the “liquid phase” are similar. However, as the volume of acidic condensate, resulting from the exposure of the film to the vapors of nitric acid, is extremely low, the driving forces leading to the delamination of the nanomesh are strongly reduced.

For simplicity, in the rest of the article, a single micropatch of nanoporous gold is denoted as “micro-domain”. As mentioned previously, after vapor dealloying, the micro-domains are separated by cracks (Fig. S3) which lead to an insulating layer. Moving the layer from insulator to conductor requires an assembling procedure where the micro-domains have to percolate together to form a single and continuous nanomesh electrode. For this purpose, after vapor dealloying, the sample is dipped in deionized water to disengage the micro-domains from the glass substrate (Fig. 1d) and at the same time dissolve copper nitrate (a byproduct of the reaction between copper and nitric acid soluble in water³²) which reduces the transparency of the electrode. One must highlight here the importance of our choice of substrate. Indeed, glass was selected as a substrate due to its weak adhesion with gold allowing a facile removal of the nanomesh from the substrate when dipped in deionized water.³³ In another word, replacing gold by another element could lead to a high adhesion to glass and will result in a failure of the transfer of the nanomesh.³⁴ The same problem can be encountered if the glass is replaced by another substrate exhibiting a high adhesion with gold such as PET (see supporting information 1).

During the procedure of dipping the glass substrate covered by the gold separated micro-domains in deionized water, the latter has the ability to float on the water surface while keeping a perfect organization (Fig. 1d). The hydrophobic aspect of the nanomeshes is the driving force allowing them to float at the air/water interface.⁵ One must point out that by replacing water by ethanol, the micro-domains quickly agglomerate in the solution (SM6). It can be concluded that the surface tension of the solution is a key parameter that must be considered carefully to successfully peel-off the micro-domains from the glass substrate and transfer them onto the liquid surface. Then, the micro-domains floating on the water surface are collected on a flexible substrate, i.e., PET (Fig. 1e) or glass (Fig. S4) where they percolate during the transfer and form an interconnected network of nanoligaments constituting the nanomesh electrode (Fig. 1f). Use of glass substrate of 24×40 mm allows the creation of nanomesh electrode of 20×30 mm. After transfer, the micro-domains become physically percolated creating a continuous nanomesh structure with some fractures (Fig. 1g). The long-range capillary attraction and short-range electrostatic repulsion act simultaneously during the assembling phase at the air/water interface, yielding in cohesion forces between the mono-domains.³⁵

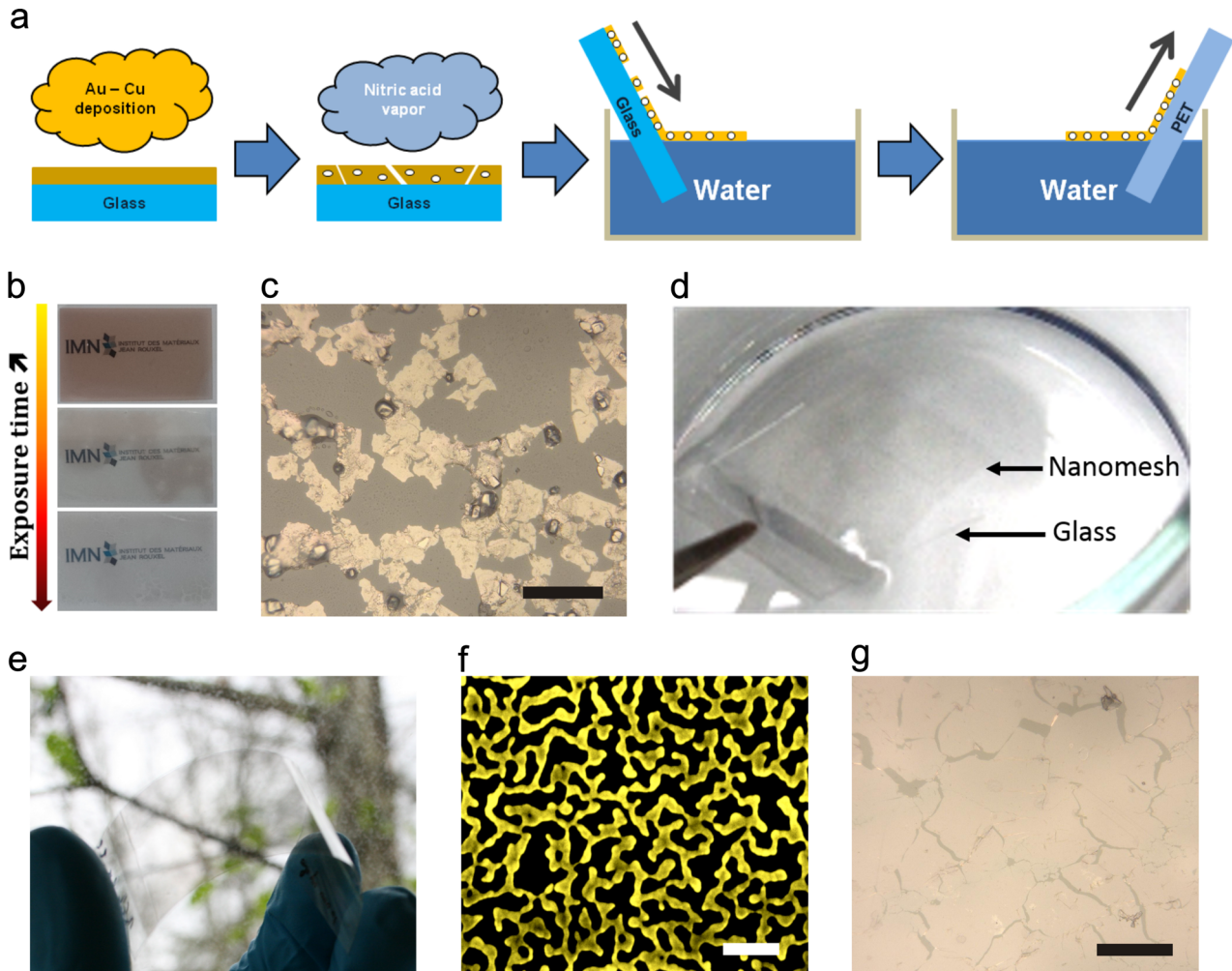


Fig. 1 Fabrication and transfer of the highly flexible gold nanomesh electrode. **a** Schematic showing the different steps of the approach used to fabricate the gold nanomesh electrode. Au-Cu ultra-thin film is first deposited by magnetron co-sputtering on a glass substrate. The alloy is then exposed to nitric acid vapors before transfer to a target flexible substrate (e.g., PET). **b** Photographs showing the evolution of the Au-Cu film as a function of exposure time to nitric acid vapors. **c** Optical microscope images of micropatches constituted of gold nanomesh on a glass substrate for a sample with 23 at.% of gold and 10 nm at initial state before transfer. **d** Photograph showing a gold nanomesh floating on the surface of distilled water and ready for the transfer onto a flexible substrate. **e** Photograph of a gold nanomesh on a PET substrate. **f** Top-view false-colors SEM image of a gold nanomesh prepared using Au-Cu film with an initial Au content of 17 at.% and a thickness of 10 nm. **g** Optical microscope images of a gold nanomesh on a glass substrate for a sample with 23 at.% of gold and 10 nm at initial state after transfer. White scale bar: 200 nm. Black scale bar: 100 μm

To modify the properties of the nanomesh and achieve the best optoelectronic performances, the thickness and the density of the nanoligaments were tuned by adjusting the (i) the gold content within the Au-Cu alloy between 11 and 23 at.%, (ii) the thickness of the ultra-thin films between 5 and 20 nm and (iii) the exposure time to nitric acid vapor to 15 and 120 min. The gold content ranges were defined according to the previous study on the thin film in order to avoid passivation of the surface observed during dealloying by free corrosion.³² It should be noted that whatever the conditions are, at first the dealloying time was fixed to 120 min allowing obtaining highly porous micro-domains containing less than 6 at.% of copper residue. Based on a set of experiments (Figs S5 and S6), we concluded that to reach the best optoelectronic performances, the Au-Cu films thickness must be 5 nm whereas the initial gold content within the alloy must be 17 at.% (Condition 1 presented in Fig. 2a). In such a case, the nanomesh electrodes showed a high transmittance (Fig. 2b), but stayed, however, limited in sheet resistance. The Haacke's figure of merit reaches $1.58 \times 10^{-3} \Omega^{-1}$ for this condition. To explore if whether such limitation originates from a poor percolation between the micro-

domains or from the structure of the nanoligaments, the sheet resistance of an isolated micro-domain of a nanomesh prepared from an Au-Cu film with 17 at.% of Au and 5 nm in thickness (Condition 1) was measured using the four probes method (Fig. 2c). Taking into account the geometry of the micro-domain and the measured resistance (i.e., 143 Ω) we evaluate a sheet resistance of about $100 \Omega \square^{-1}$ which is almost equal to the sheet resistance measured on the macroscale ($96 \Omega \square^{-1}$). This result indicates that the limitation in sheet resistance is clearly related to the characteristics (i.e., structure, thickness, pore size, Cu residue concentration, etc) of the micro-domains rather than their organization on the macroscale.

To further decrease the sheet resistance of the nanomeshes, the exposure time of the Au-Cu films to acidic vapors was adjusted to tune the morphology and copper residue in the nanoligaments. Indeed, the dissolution of the copper atoms by nitric acid with the dealloying time leads to the evolution of the nanoporous architecture. At an early dealloying stage, only tiny isolated holes are observed within the structure due to the huge amount of copper atoms remaining in the film.³² Similarly to dealloying in

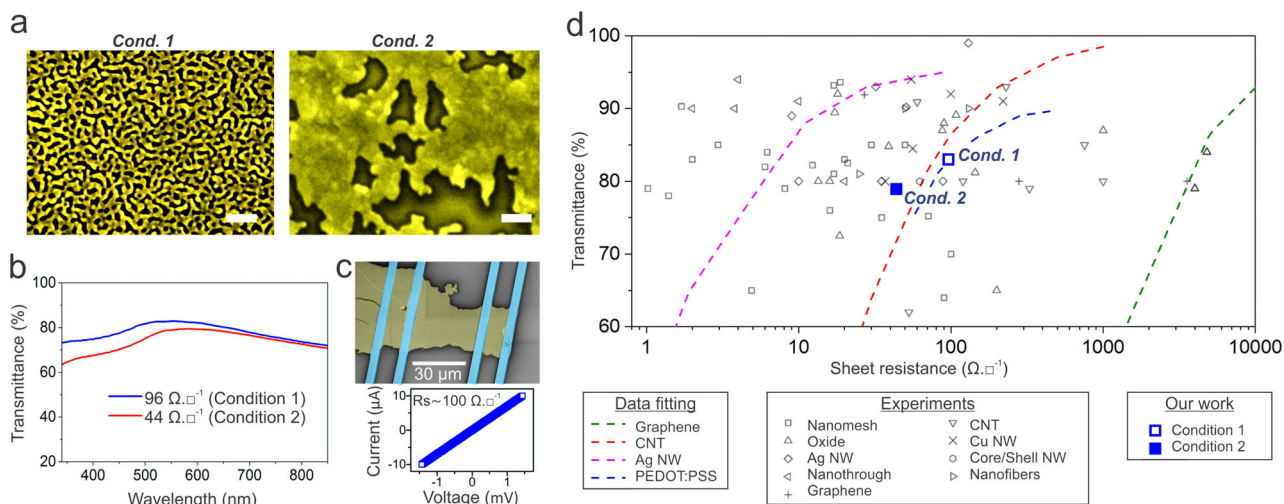


Fig. 2 Morphology and optoelectronic properties of the Au nanomesh electrodes. **a** Top-view SEM images showing two examples of the typical morphologies of gold nanomeshes prepared using Au-Cu ultra-thin films with 17 at.% of initial gold content and 5 nm initial thickness with different exposure time: (condition 1) 120 min acidic exposure and (condition 2) 15 min acidic exposure. Scale bar: 200 nm. **b** Example of two UV-Vis transmission spectra of Au nanomesh electrodes on PET with the different values of sheet resistance; the spectra show relatively flat curves for the entire visible wavelength range. **c** False-colors SEM image of four terminal electrical conductivity measurement of a single micro-domain and the corresponding I-V curve recorded at room temperature; the yellow and cyan colors represent the gold nanomesh and the platinum electrodes, respectively. **d** Optical transmission at 550 nm versus sheet resistance of Au nanomesh electrodes on PET prepared with 17 at.% initial gold content and 5 nm initial thickness with different exposure time: 15 min (solid square—condition 2) and 120 min (hollow square—condition 1). For the purpose of comparison, the optoelectronic performances of PEDOT:PSS, carbon nanotubes, graphene, silver nanowires, nanotroughs, copper nanowires, core/shell nanowires, nanofibers, oxide, and other nanomeshes are also included on the graph. – Inspired by reviews^{2,15} – The full list of references used in this figure is provided in Supporting Information. Note that the transmittance presented in the graph does not include the transmittance of the substrate

the liquid phase, the kinetic of the vapor dealloying process was found to increase as decreasing the gold content in the alloy. In this part, a sample with 5 nm in initial thickness and with 17 at.% of Au was used. Nanomeshes with ~17 at.% of Cu residue were obtained for an exposure time of 15 min. For this sample (Condition 2 in Fig. 2a), the sheet resistance decreased sharply from 96 to 44 $\Omega\text{□}^{-1}$ while maintaining a high transparency (the transmittance slightly decreases from 83 to 79%). This nanomesh shows the highest Haacke's figure of merit of $2.13 \times 10^{-3} \Omega^{-1}$. Contrary to metal thin films with a thickness exceeding 20 nm which exhibit usually a very low transmittance,^{2,36} these nanomeshes are found to be highly transparent. In Fig. 2d the transmittance at 550 nm is plotted as a function of the sheet resistance R_s of these nanomesh electrodes on PET for 17 at.% of gold content and different exposure times to nitric acid vapors (15 and 120 min). For the purpose of comparison, the optoelectronic performances of other technologies (e.g., carbon nanotubes (CNTs), graphene, silver nanowires) extracted from the literature are also presented in the same figure. The optoelectronic performances of these nanomeshes are comparable to the ones based on graphene, CNTs, PEDOT:PSS, silver nanowires as well as nanomeshes fabricated with other approaches (Fig. 2d).^{3,9,18} However, the sheet resistance of the nanomeshes studied in this paper is slightly higher than the ones obtained in some other studies. Most probably, such high values originate from the size of the ligament that are smaller (much lower than 1 micrometer) than the one reported in the literature for lowest sheet resistance (few micrometers).^{37,38} On the other hand, gold nanomesh structures reported in the literature with the same ligaments size exhibit equivalent optoelectronic performances.³⁹ Transmittance of the nanomeshes presented in this study is the same order of magnitude than other approaches develop for FTCE (between 80 and 90%). It is important to stress that the comparison of performances given in Fig. 2d does not take into account all the other important performances required for an industrial FTCE application: ability for deposition on large surface area, simplicity

and high efficiency of the deposition process. Another very important property to be studied is the ability of FTCE to be adapted to flexible films. It is the reason why the evolution of the sheet resistance of the nanomeshes deposited on PET films has been studied as a function of the bending radius of the PET films.

To examine the mechanical durability of the nanomesh electrodes on PET substrate, bending tests were carried out (Fig. 3). For these experiments, we selected the nanomeshes prepared with Au-Cu films with 17 at.% of Au and a thickness of 5 nm. This nanomesh exhibits a sheet resistance of 44 $\Omega\text{□}^{-1}$ and a transparency of 79% before the mechanical test (Condition 2). For the sake of comparison, such mechanical tests were also performed on Au-Cu alloy thin film in the same experimental conditions. As it can be seen, even under extreme deformation conditions (positive strain up to 2.5%), the nanomesh remains conductive (Fig. 3a–c). While the electrical resistance of the nanomesh, plotted as a function of the bending radius, shows no obvious modification, the one of the Au-Cu film used as a reference sharply increases during the deformation (Fig. 3d). For comparison, the electrical resistance of an ITO thin film deposited on PET substrate was found to strongly increase until 2000% for a bending radius of 10 mm (positive strain of 1%).¹⁵ This experiment is a direct proof of the highly resistant aspect of our nanomesh electrodes to mechanical deformation. We attribute this behavior to the special structure of the micro-domains constituting the electrode which allows the material to adapt its shape against the external mechanical stimulation; this is related to the fact that the ligaments could be considered as a one dimension nanoobject with a freedom to adapt themselves to the deformation in a two dimensions space, the substrate surface (not possible in case of a continuous film)⁵ or even in a three dimensions space. The mechanical stability of the electrode was further explored under severe and repeated positive deformations. For this purpose, the electrodes were bent up for 10,000 times (Fig. 3e). During each cycle, the electrode was bent up until reaching a radius of 6 mm. The electrical resistance of the nanomesh electrode, measured after each bending cycle, showed a relatively stable behavior (the resistance

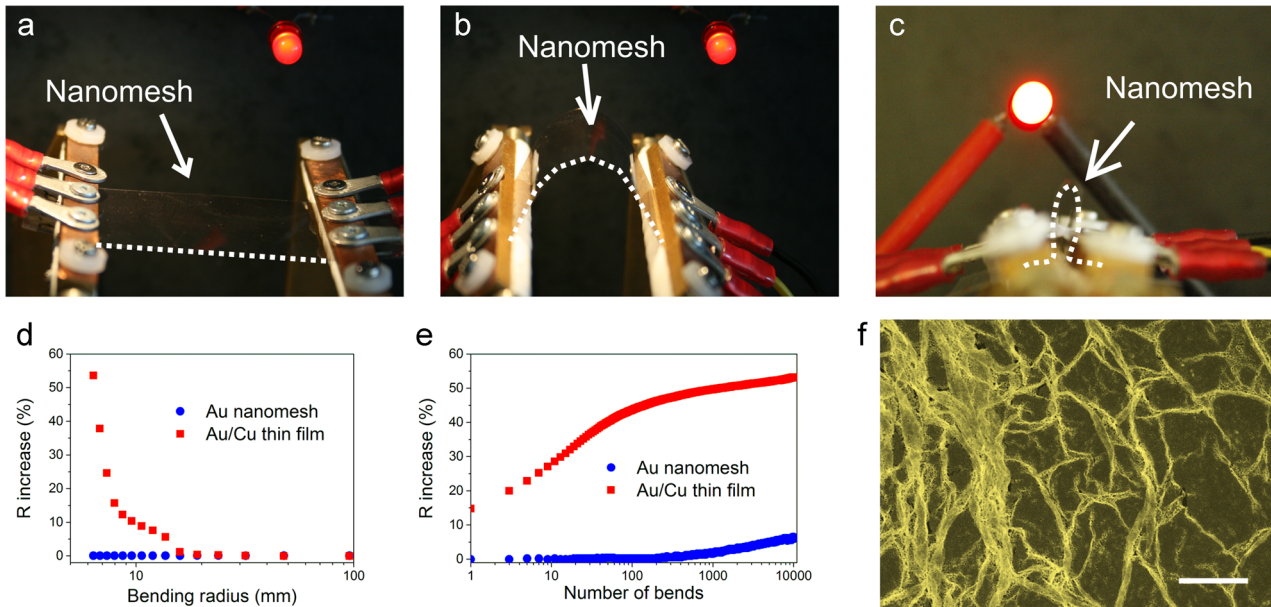


Fig. 3 Mechanical properties of the nanomesh electrodes. **a–c** Photographs of nanomesh electrode on flexible PET substrate. The current through the nanomesh switches on the LED **a** before strain, **b** with $\epsilon = 1.2\%$ and **c** with $\epsilon = 2.5\%$. **d** Increase of sheet resistance versus bending radius for bendable transparent electrodes consisting of gold nanomesh networks, for 5 nm Au-Cu film with 17 at.% of Au on PET substrate. **e** Variation in resistance of the gold nanomesh electrode and Au-Cu film on PET film as a function of the number of cycles of repeated bending to a radius of 6 mm. **f** Typical SEM images of nanomesh after 10,000 bending cycles. The SEM images are representative of nanomesh bend after 10,000 cycles. White scale bar: 5 μm

increase only by 7%) compared to the Au-Cu reference for which the resistance increase by 54%. The increase in resistance of our nanomeshes observed after 10,000 cycles (i.e., 7%) is extremely low compared to ITO films on PET (an increase of about 2200% in the resistivity after bending to a radius of 20 mm for more than 20 times).¹⁵ When examined by SEM after 10,000 of bending cycles, the nanomesh was found to be locally folded in some regions (Fig. 3f). This special folding ability of nanoligaments is the key point allowing the nanomesh to overcome the extremely high stress generated during the severe mechanical deformations.

DISCUSSION

In summary, an original process based on vapor dealloying was developed in order to create nanomesh electrodes with very good optoelectronic properties as flexible transparent conductor. Nanomesh with a resistivity of $44 \Omega \square^{-1}$ and a transmittance of 79% leading to a Haacke factor of merit of $2.13 \times 10^{-3} \Omega^{-1}$ are created with remarkable stability against mechanical deformations (7% increase of resistance after 10,000 cycles at 1% strain). The process allowed also a simple transfer on the complex surface and different substrates such as tubular glass (Fig. S4) or flat polymer substrates. Future works should focus on the use of carbon nanotubes or graphene combined with these nanomeshes in order to decrease the sheet resistance of these transparent flexible membranes. Moreover, the next stage should be a scale up to these nanomeshes with larger sizes for screen devices of few centimeters square.

METHODS

Growth of Au-Cu alloy thin film

The Au-Cu thin film, used to prepare the Au nanomesh, were synthesized by DC co-sputtering in pure argon plasma of an Au (diameter: 76.2 mm; purity: 99.99%) and a Cu (diameter: 76.2 mm; purity: 99.99%) targets in a co-focal geometry. The distance between the targets and the substrate was 130 mm. The deposition of the Au-Cu thin film was then carried out at an Ar plasma pressure of 0.5 Pa without applying any intentional heating to the substrate. For all the depositions, the base pressure was less than 4×10^{-5} Pa.

In order to control the composition of the thin film, the electrical power applied to the Cu target was fixed to 300 W whereas the one applied to the Au target was tuned. Three electrical powers applied to the Au target were selected (30, 50, and 70 W) allowing growing ultra-thin film with 11, 17, and 23 at.% of Au, respectively. Moreover, three deposition times were selected to tune the initial thickness of the as-grown thin film (5 s, 10 s and 20 s) allowing growing thin film with 5, 10 and 20 nm, respectively.

Vapor dealloying and nanomesh transfer

The Au-Cu thin film deposited on glass substrate with a size of 24×40 mm was placed in a crystallizer, with 100 mm in diameter and 15 mm in height, containing nitric acid without contact with the solution. Sample is set at 5 mm from the liquid front. Nitric acid at 16 mol L^{-1} was provided by Carlos Erba. The amount of nitric acid was fixed to 20 mL. An air flow was used in order to force the vapor to condense on the sample surface. The dealloying time was tuned between 15 and 120 min. To stop the dealloying process, the sample was taken away from the nitric acid vapors and dried in ambient air for 5 min. Then, the sample was immersed in distilled water to transfer the nanomesh. The nanomesh was left floating on the distilled water surface for 5 min before the transfer to allow dissolving the $\text{Cu}(\text{NO}_3)_2$ residue. The nanomesh was transferred onto polyethylene terephthalate (PET) substrate with a thickness of 0.125 mm.

Characterization

The SEM images were recorded using a JEOL JSM 7600F microscope operating at 5 kV. The AFM images were recorded using a NanoWizard 3 from JPK instruments. The X-ray photoemission spectroscopy (XPS) measurements were carried out on an AXIS Nova from Kratos using a monochromatic Al K α X-ray source (1486.6 eV). The spectra were recorded with a pass energy of 20 eV. Optical images were recorded using a VHX-5000 from Keyence. For the electrical conductivity measurement of a single micro-domain, nanomesh was sonicated and deposited onto an oxidized silicon substrate. Then they were examined under SEM and focused ion beam induced platinum deposition was made using beam with 30-kV acceleration voltage and current of 80–430 pA with an FEI Helios NanoLab 650 instrument. The thickness of the deposition was roughly 0.5 μm . The sheet resistances of the films were measured using a digital multimeter (Keithley 2401) with a four-point probe configuration to avoid contact resistance. Stretching experiments were conducted with a homemade setup (Fig. S9), and meanwhile, the resistance was measured by a two-probe method.

DATA AVAILABILITY

All experimental data generated or analyzed during this work are included in the article and the Supplementary Information Files.

ACKNOWLEDGEMENTS

The authors gratefully acknowledge F. Petitgas (IMN, Nantes) and N. Stephant (Nantes University) for their technical assistance on the co-sputtering system and on the SEM, respectively. The authors gratefully acknowledge N. Langlois (Nantes University) and B. Angleraud (Polytech Nantes) for their technical assistance on the AFM. The authors gratefully acknowledge T. Devie (IMN, Nantes), E. Kamba and M. Gicquel for the design and build of the testing bench. The research was performed within the frame of COST Action MP1202 (HINT) "Rational Design of Hybrid Interfaces". The COST action MP1202 (HINT) is acknowledged for providing funding for ECOST-STSM-MP1202-031015-067653 grant that contributed to this research project.

AUTHOR CONTRIBUTIONS

A.-A. El Mel designed the vapor dealloying experiment and nanomesh transfer. A. Chauvin. and W. Txia Cha Heu conducted the film deposition, vapor dealloying experiments, nanomesh transfer, and film characterization. J. Buh conducted ion-beam-induced platinum deposition and electrical conductivity measurement of single micro-domain. A.-A. El Mel proposed and directed the experiments. A.-A. El Mel and P.-Y. Tessier co-supervised the project. A. Chauvin, A.-A. El Mel, and P.-Y. Tessier co-wrote the paper. All authors discussed the results and worked on the manuscript.

ADDITIONAL INFORMATION

Supplementary information accompanies the paper on the *npj Flexible Electronics* website (<https://doi.org/10.1038/s41528-019-0049-1>).

Competing interests: The authors declare no competing interests.

Publisher's note: Springer Nature remains neutral with regard to jurisdictional claims in published maps and institutional affiliations.

REFERENCES

1. *Handbook of Transparent Conductors*. (Springer US 2011).
2. Ellmer, K. Past achievements and future challenges in the development of optically transparent electrodes. *Nat. Photonics* **6**, 809–817 (2012).
3. Kim, K. et al. Stretchable and transparent electrodes based on in-plane structures. *Nanoscale* **7**, 14577–14594 (2015).
4. Kumar, A. & Zhou, C. The race to replace tin-doped indium oxide: which material will win? *ACS Nano* **4**, 11–14 (2010).
5. Guo, C. F., Sun, T., Liu, Q., Suo, Z. & Ren, Z. Highly stretchable and transparent nanomesh electrodes made by grain boundary lithography. *Nat. Commun.* **5**, 3121–3128 (2014).
6. Jang, H. Y., Lee, S.-K., Cho, S. H., Ahn, J.-H. & Park, S. Fabrication of metallic nanomesh: Pt nano-mesh as a proof of concept for stretchable and transparent electrodes. *Chem. Mater.* **25**, 3535–3538 (2013).
7. Tahar, R. B. H., Ban, T., Ohya, Y. & Takahashi, Y. Tin doped indium oxide thin films: electrical properties. *J. Appl. Phys.* **83**, 2631 (1998).
8. Cheng, T., Zhang, Y., Lai, W.-Y. & Huang, W. Stretchable thin-film electrodes for flexible electronics with high deformability and stretchability. *Adv. Mater.* **27**, 3349–3376 (2015).
9. De, S. et al. Silver nanowire networks as flexible, transparent, conducting films: extremely high DC to optical conductivity ratios. *ACS Nano* **3**, 1767–1774 (2009).
10. Hu, L., Wu, H. & Cui, Y. Metal nanogrids, nanowires, and nanofibers for transparent electrodes. *Mrs. Bull.* **36**, 760–765 (2011).
11. Garnett, E. C. et al. Self-limited plasmonic welding of silver nanowire junctions. *Nat. Mater.* **11**, 241–249 (2012).
12. Wu, Z. Transparent, conductive carbon nanotube films. *Science* **305**, 1273–1276 (2004).
13. Bonaccorso, F., Sun, Z., Hasan, T. & Ferrari, A. C. Graphene photonics and optoelectronics. *Nat. Photonics* **4**, 611–622 (2010).
14. Kim, K. S. et al. Large-scale pattern growth of graphene films for stretchable transparent electrodes. *Nature* **457**, 706–710 (2009).
15. Wu, H. et al. A transparent electrode based on a metal nanotrough network. *Nat. Nanotechnol.* **8**, 421–425 (2013).
16. An, B. W. et al. Stretchable and transparent electrodes using hybrid structures of graphene–metal nanotrough networks with high performances and ultimate uniformity. *Nano. Lett.* **14**, 6322–6328 (2014).
17. Kirchmeyer, S. & Reuter, K. Scientific importance, properties and growing applications of poly(3,4-ethylenedioxythiophene). *J. Mater. Chem.* **15**, 2077 (2005).
18. Kim, Y. H. et al. Highly conductive PEDOT:PSS electrode with optimized solvent and thermal post-treatment for ITO-free organic solar cells. *Adv. Funct. Mater.* **21**, 1076–1081 (2011).
19. Guo, C. F. & Ren, Z. Flexible transparent conductors based on metal nanowire networks. *Mater. Today* **18**, 143–154 (2015).
20. Khan, A. et al. High-performance flexible transparent electrode with an embedded metal mesh fabricated by cost-effective solution process. *Small* **12**, 3021–3030 (2016).
21. Kim, H.-J. et al. High-durable AgNi nanomesh film for a transparent conducting electrode. *Small* **10**, 3767–3774 (2014).
22. Voronin, A. S. et al. High performance hybrid rGO/Ag quasi-periodic mesh transparent electrodes for flexible electrochromic devices. *Appl. Surf. Sci.* **364**, 931–937 (2016).
23. Hong, S. et al. Nonvacuum, maskless fabrication of a flexible metal grid transparent conductor by low-temperature selective laser sintering of nanoparticle ink. *ACS Nano* **7**, 5024–5031 (2013).
24. Kim, H.-J. et al. Highly efficient and stable cupronickel nanomesh electrode for flexible organic photovoltaic devices. *J. Power Sources* **331**, 22–25 (2016).
25. Lu, Z. et al. Three-dimensional bicontinuous nanoporous materials by vapor phase dealloying. *Nat. Commun.* **9**, 276–282 (2018).
26. Pickering, H. W. & Swann, P. R. Electron metallography of chemical attack upon some alloys susceptible to stress corrosion cracking. *Corros. - Natl. Assoc. Corros. Eng.* **19**, 373t–389t (1963).
27. Sun, S., Chen, X., Badwe, N. & Sieradzki, K. Potential-dependent dynamic fracture of nanoporous gold. *Nat. Mater.* **14**, 894–898 (2015).
28. Dotzler, C. J. et al. In situ observation of strain development and porosity evolution in nanoporous gold foils. *Adv. Funct. Mater.* **21**, 3938–3946 (2011).
29. Erlebacher, J. & Ding, Y. Method of forming nanoporous membranes. 1–8 (2004).
30. Erlebacher, J., Aziz, M. J., Karma, A., Dimitrov, N. & Sieradzki, K. Evolution of nanoporosity in dealloying. *Nature* **410**, 450–453 (2001).
31. McCue, I., Benn, E., Gaskey, B. & Erlebacher, J. Dealloying and dealloyed materials. *Annu. Rev. Mater. Res.* **46**, 1.1–1.24 (2016).
32. El Mel, A.-A. et al. Unusual dealloying effect in gold/copper alloy thin films: the role of defects and column boundaries in the formation of nanoporous gold. *ACS Appl. Mater. Interfaces* **7**, 2310–2321 (2015).
33. Ciesielski, P. N. et al. Functionalized nanoporous gold leaf electrode films for the immobilization of photosystem I. *ACS Nano* **2**, 2465–2472 (2008).
34. Pask, J. A. & Fulrath, R. M. Fundamentals of glass-to-metal bonding: viii, nature of wetting and adherence. *J. Am. Ceram. Soc.* **45**, 592–596 (1962).
35. Retsch, M. et al. Fabrication of large-area, transferable colloidal monolayers utilizing self-assembly at the air/water interface. *Macromol. Chem. Phys.* **210**, 230–241 (2009).
36. Ghosh, D. S., Martinez, L., Giurgola, S., Vergani, P. & Pruneri, V. Widely transparent electrodes based on ultrathin metals. *Opt. Lett.* **34**, 325–327 (2009).
37. Kiruthika, S., Rao, K. D. M., Kumar, A., Gupta, R. & Kulkarni, G. U. Metal wire network based transparent conducting electrodes fabricated using interconnected crackled layer as template. *Mater. Res. Express* **1**, 026301 (2014).
38. Gong, S. et al. Fabrication of highly transparent and flexible nanomesh electrode via self-assembly of ultrathin gold nanowires. *Adv. Electron. Mater.* **2**, 1600121 (2016).
39. Ho, M. D., Liu, Y., Dong, D., Zhao, Y. & Cheng, W. Fractal gold nanoframework for highly stretchable transparent strain-insensitive conductors. *Nano. Lett.* **18**, 3593–3599 (2018).



Open Access This article is licensed under a Creative Commons

Attribution 4.0 International License, which permits use, sharing, adaptation, distribution and reproduction in any medium or format, as long as you give appropriate credit to the original author(s) and the source, provide a link to the Creative Commons license, and indicate if changes were made. The images or other third party material in this article are included in the article's Creative Commons license, unless indicated otherwise in a credit line to the material. If material is not included in the article's Creative Commons license and your intended use is not permitted by statutory regulation or exceeds the permitted use, you will need to obtain permission directly from the copyright holder. To view a copy of this license, visit <http://creativecommons.org/licenses/by/4.0/>.

© The Author(s) 2019